

Determination of Tube Output (kVp) and Exposure Mode for Breast Phantom of Various Thicknesses/Glandularity for Digital Mammography

Kamal IZDIHAR¹, Kumari Chelliah KANAGA¹, Vijayalakshimi KRISHNAPILLAI², Tamanang SULAIMAN³

Submitted: 24 Jun 2014

Accepted: 20 Nov 2014

¹ Diagnostic Imaging and Radiotherapy Programme, Faculty of Health Sciences, University Kebangsaan Malaysia, Jalan Raja Muda Abdul Aziz, 50300, Kuala Lumpur, Malaysia

² Diagnostic Imaging Department, Hospital Tengku Ampuan Rahimah, Jalan Langat, 41200 Klang, Selangor, Malaysia

³ The National Cancer Society of Malaysia, Women's Cancer Detection and Breast Clinic, 66 Jalan Raja Muda Abd Aziz, 50300 Kuala Lumpur, Malaysia

Abstract

Background: Optimisation of average glandular dose (AGD) for two-dimensional (2D) mammography is important, as imaging using ionizing radiation has the probability to induce cancer resulting from stochastic effects. This study aims to observe the effects of kVp, anode/filter material, and exposure mode on the dose and image quality of 2D mammography.

Methods: This experimental study was conducted using full-field digital mammography. The entrance surface air kerma was determined using thermoluminescent dosimeter (TLD) 100H and ionization chamber (IC) on three types of Computerized Imaging Reference System (CIRS) phantom with 50/50, 30/70, and 20/80 breast glandularity, respectively, in the auto-time mode and auto-filter mode. The Euref protocol was used to calculate the AGD while the image quality was evaluated using contrast-to-noise ratio (CNR), figure of merit (FOM), and image quality figure (IQF).

Results: It is shown that AGD values in the auto-time mode did not decrease significantly with the increasing tube voltage of the silver filter ($r = -0.187$, $P > 0.05$) and rhodium filter ($r = -0.131$, $P > 0.05$) for all the phantoms. The general linear model showed that AGD for all phantoms had a significant effect between different exposure factors [$F(6,12.3) = 4.48$ and mode of exposure $F(1,86) = 4.17$, $P < 0.05$, respectively] but there is no significant difference between the different anode/filter combination [$F(1,4) = 0.571$].

Conclusion: In summary, the 28, 29, and 31 kVp are the optimum kVp for 50%, 30%, and 20% breast glandularity, respectively. Besides the auto-filter mode is suitable for 50%, 30%, and 20% breast glandularity because it is automatic, faster, and may avoid error done by the operator.

Keywords: radiation dose, CDMAM, digital mammography

Introduction

Many mammography systems are supplied with the ability to automatically select a beam quality tailored and use manually set tube potential and target filter. It is well known from a theoretical consideration that the optimal energy is different for breasts of different sizes and compositions. The optimum spectrum for mammography requires a compromise between image contrast (maximised with lower energies), radiation dose (minimised), image statistical noise (minimised) with a higher incident exposure to the detector, and constraints on tube loading or maximum exposure time (1).

The optimised anode/filter combination in digital mammography, with the highest image quality and the lowest possible average glandular dose, can be evaluated in the following manner. A technical image quality evaluation included phantom images, signal to-noise (SNR), and contrast-to-noise (CNR) analysis together with average glandular dose information (1). A relatively new concept in assessing the performance of digital mammography systems is that of the figure-of-merit (FOM) and the image quality figure (IQF) value using the contrast detail mammography (CDMAM) phantom. The IQF is the parameter used to calculate the image quality taking into account the contrast

and detail resolution of the image analysed. The contrast-detail curve is useful as a measure of the image quality too, because it is a graphical representation in which the whole thickness and diameter are plotted for each contrast-detail combination detected in the radiographic image of the phantom (2).

An FOM has been used to compare techniques and exposure factors in the optimization of mammography systems; (3,4,5) thus, it has been used to compare the performance of similar digital mammography systems employing different spectra (6) and has also been more rarely used to compare different digital mammography systems.

A critical factor determining both image quality and dose is the spectral composition of the X-ray beam. The energy spectrum is determined primarily by the tube target material, the amount and type of internal and external filtration, and the tube's operating voltage (the kVp). Clinical trials and scientific investigations have found that a tungsten X-ray tube with rhodium (Rh) and silver (Ag) filters is optimal to be used in digital mammography for all breast thicknesses and will allow for important dosage reductions in the order of 30% while maintaining an excellent image quality (7).

The objective of the study is to observe the effects of kVp, anode/filter material, and exposure mode on the dose and image quality for two-dimensional mammography.

Materials and Methods

The experiment was conducted at the Breast Clinic using Hologic Selenia dimensions full-field digital mammography (Hologic, Bedford, United States). Full-field digital mammography (FFDM) with AWS 5000 is equipped with a Tungsten (W) anode X-ray tube, with a choice of Rh or Ag filtration (50 mm thick, each). The Selenia Dimensions from Hologic use TFT-based Direct Capture Technology-based detectors overlaid with amorphous selenium. The pixel matrix is 3328×4096 pixels with a pixel pitch of $70 \mu\text{m}$ for a 24×29 cm active image area. The Selenia Dimensions has four modes of automatic exposure control: auto-filter, auto-KV, auto-time, and thickness equivalent control.

Figure 1a shows three types of phantoms used for this experiment. The average elemental composition of the human breast being mimicked is based on the individual elemental composition of adipose and glandular tissue as reported by Hammerstein et al. (8). The first phantom composed of 20% glandular and 80% adipose

tissue of tissue equivalent breast phantom (Breast phantom, Computerized Imaging Reference Systems (CIRS), Norfolk, Virginia) with 6 cm thickness, the second phantom 30/70 with 5-cm thickness, and the third phantom is 50/50 with 4 cm thickness. CIRS resin material mimics the photon attenuation coefficients of a range of breast tissues. In each phantom stack assembly, the signal block contains spec groups (0.13 to 0.40 mm in diameter) that simulate microcalcification, nylon fibers (0.30 to 1.25 mm) that simulate fiber, and hemispheric masses (0.90 to 4.76 mm in thickness) that simulate masses. Test objects within the phantom range in size from objects that should be visible on any system to those that would be difficult to resolve even on the best mammographic system are available today.

Acquisition of mammograms was undertaken with two parameters: first with automatic exposure control (AEC or auto-filter) and second with the auto-time mode; the system selected

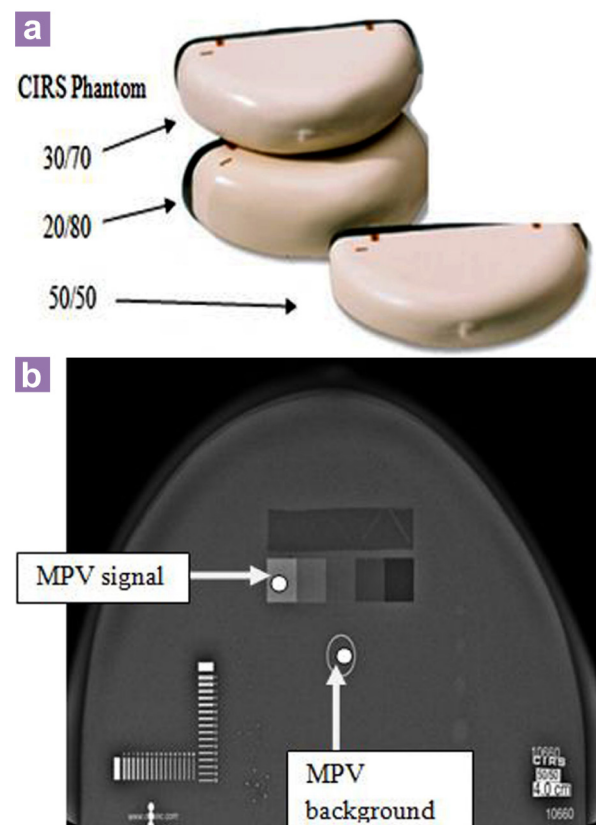


Figure 1: (a) Three types of CIRS breast phantoms used in this research, (b) The MPV signal and MPV background were measured at that particular area on the CIRS phantom.

the mAs, whereas the operator selected the filter and kVp manually. There are two types of filters used (Argentum and Rh), with each filter being exposed to 26, 28, 30, 32, and 34kVp, respectively. Both exposures were made with craniocaudal projection, with the phantoms positioned at the chest wall edge of the receptor, centered left to right, with the source to image distance of 65 cm, the focal spot size broad, and the compression force of 10 N.

The method describe in International Atomic Energy Agency (IAEA) TRS 457 for the assessment of the dose was followed (9). Thermoluminescent dosimeter 100-H (TLD-100H) was placed on top of the phantom to measure the entrance surface air kerma (ESAK) (Figure 2a). The half value layer (HVL) for each beam quality was measured using an ionization chamber (Model 9095 Radcal Corporation) with the compression paddle as described in the same report (TRS 457). TLDs were calibrated in terms of air kerma at mammographic energies, using all anode/filter combination as used in normal practice. An ionization chamber was used to calibrate TLDs (Figure 3). The ionization chamber was placed at the same effective point of the measurements and exposed to the same dose as TLDs so that the energy responses were consistent because it was calibrated at the same energies where the measurements were taken (10).

The experiment was repeated using the calibrated ionization chamber (Radcal 9095, Radcal Corporation, Monrovia, California, USA) with the same exposure parameters. The phantom was removed and the ionization chamber was placed on the reference point of the radiation detector at the mammographic reference point, 45 mm above the cassette table and 40 mm from the chest wall edge and centered with respect to the lateral direction (Figure 2b). The compression plate was in contact with the detector. The exposures were made using the tube loading obtained from the previous experiment by International Atomic Energy Agency (IAEA) 2006. The entire experiment was repeated three times for consistency.

The AGD was calculated for each combination parameter of those settings (anode/filter combination, kVp, and mAs values) chosen by the system, by applying published conversion factors to the ESAK previously measured using the European protocol.

$$AGD = ESAK \cdot g \cdot c \cdot s \quad \text{Equation 1}$$

ESAK is the incident air kerma at the

upper surface of the breast, measured without backscatter, g-factor is the incident air kerma to the average glandular dose conversion factor,

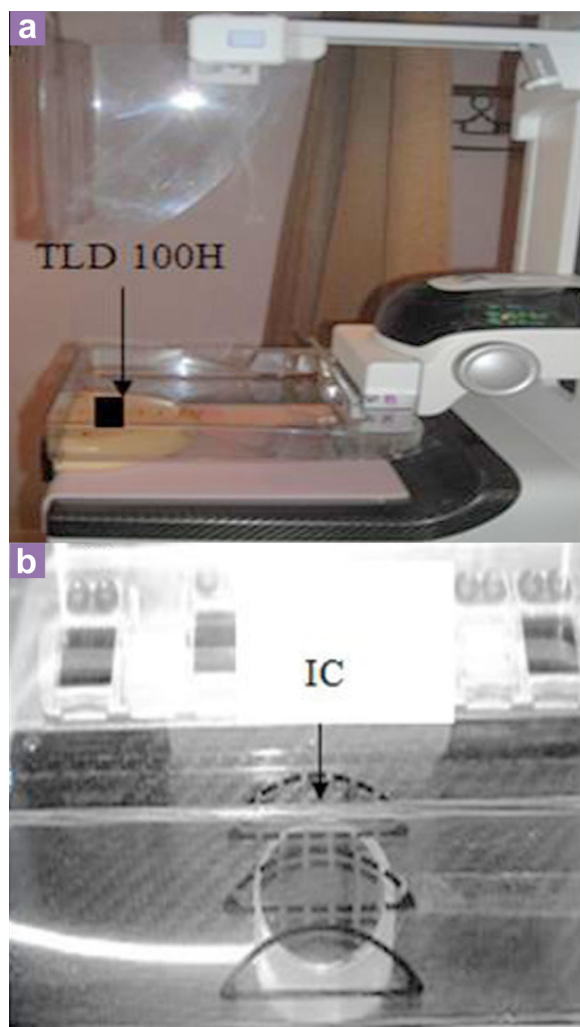


Figure 2: (a) ESAK measurement with TLD 100H on the CIRS breast phantom, (b) ESAK measurement with the ionization chamber was placed on the reference point of the radiation detector without breast phantom.

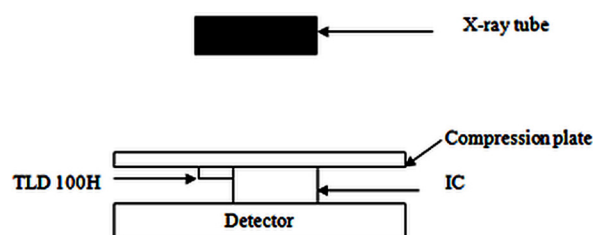


Figure 3: Calibration process of the TLD 100H with IC.

factor c corrects for any difference in breast composition from 50% glandularity, and factor s corrects for any difference due to the use of a different X-ray spectrum.

Image quality assessment

CNR was calculated according to the definition in the European guidelines for quality assurance in mammographic screening and followed the same method as Kanaga et al. (13).

$$CNR = \frac{MPV_{SIGNAL} - MPV_{BACKGROUND}}{\sqrt{\frac{SD_{SIGNAL}^2 + SD_{BACKGROUND}^2}{2}}} \quad \text{Equation 2}$$

The mean pixel value (MPV) signal was measured in an area of 100% glandularity of the step wedge (center of the step wedge), MPV background is the mean pixel value measured in the reference zone, and standard deviation (SD) signal and SD background. The size of the region of interest used was 0.8cm × 0.8cm (Figure 1b). The FOM, typically used for the optimization of tube voltage in digital systems was calculated to analyze the effectiveness of each mode of exposure.

$$FOM = \frac{CNR^2}{AGD} \quad \text{Equation 3}$$

The FOM was calculated for all acquisition conditions and plotted as a function of kV for the three phantom thicknesses. An optimal peak tube voltage was determined by taking the maximum value of the FOM for each anode/filter combination. These values were compared with those chosen by the system when operating in the auto-filter mode.

Contrast detail mammography (CDMAM)

The phantom used in this work is the CDMAM 3.4 (Artinis, Nijmegen, Netherlands) consisting of an aluminum base with gold disks of various thickness and diameters, which attaches to a plexiglas cover (Figure 4a). The gold disks range in diameter from 0.06 to 2.0 mm and in thickness from 0.03 to 2.0 μm, resulting in a radiation contrast range of 0.5–30% at standard mammography exposure conditions. Contrast detail measurements were made using a CDMAM phantom, with a 20 mm thickness of polymethylmethacrylate (PMMA) above and below the phantom. The total attenuation is equivalent to a 50 mm thickness of PMMA or a 60 mm thickness of typical breast tissue. Sets of 16 images were obtained, using exposure factor similar to that of the previous experiment.

Threshold contrasts were derived from curves fitted to the results, as described in the UK protocol (Figure 4b) (15, 16).

Statistical analysis

The general linear model was used to demonstrate a significant difference between different combination of anode/filter and tube voltage of the AGD using TLD. Pearson test was also used to see the correlation between the AGD value of TLD with different tube voltage, anode/filter combinations, and CNR. Statistical significance is deemed to occur when the P value is less than 0.05.

Results

In this study, three phantoms were used to compare the radiation dose between two different filters (Ag vs Rh) received by five different tube

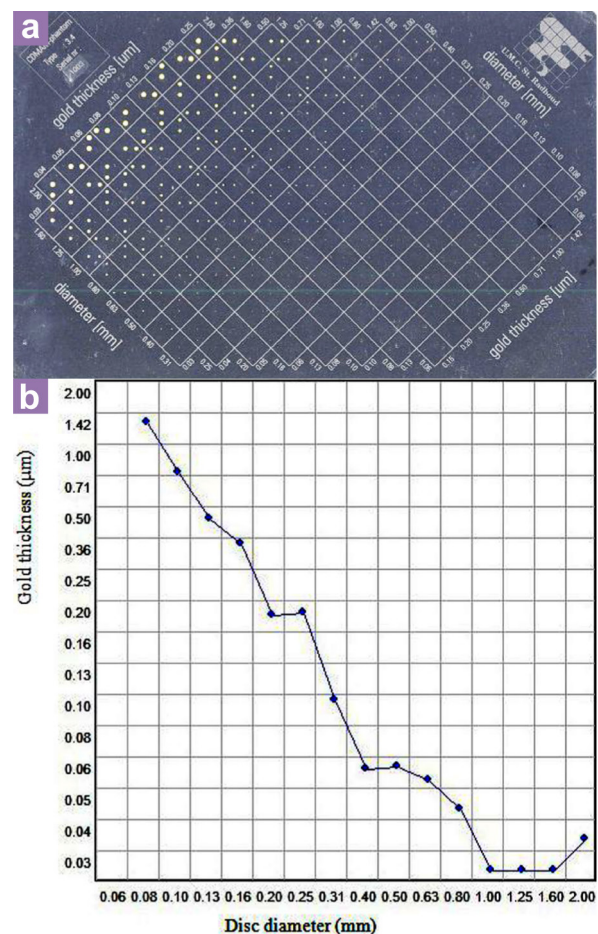


Figure 4: (a) Contrast detail mammography (CDMAM) phantom, (b) Contrast detail curve to calculate image quality figure (IQF) value automatically.

outputs (26, 28, 30, 32, and 34 kVp) in the auto-time mode (Table 1). The result was divided into three phantoms: 20/80 (6 cm), 30/70 (5 cm), and 50/50 (4 cm). The AGD value obtained from the experiment increased with thickness. The radiation dose was lower in the auto-time mode than the with auto-filter mode. All phantoms have a lower AGD with a higher kVp 32 to 34 compared with a lower kVp 26 and 28. It is shown that AGD values in the auto-time mode did not decrease significantly with the increasing tube voltage of the Ag filter ($r = -0.187$, $P > 0.05$) and Rh filter ($r = -0.131$, $P > 0.05$) for all the phantoms.

The CNR and FOM values were plotted against the tube potential for each anode/filter combination, respectively (Figures 5a–5c), (Figure 6a–6c). The CNR and FOM values are higher with a lower kVp compared with a higher kVp. Observed from figures 5a–5c and figure 6a–6c, the optimum kVp was 26 and 28, respectively. Spectrum Rh has a higher value of FOM and CNR for all phantoms. For the CDMAM phantom, the IQF value was higher with a lower kVp (28kVp) (Figure 7 and Table 2). In contrast, the IQF value was lower with 26 kVp, unlike FOM and CNR. Therefore, 26 kVp was not the optimum kVp for both spectrums.

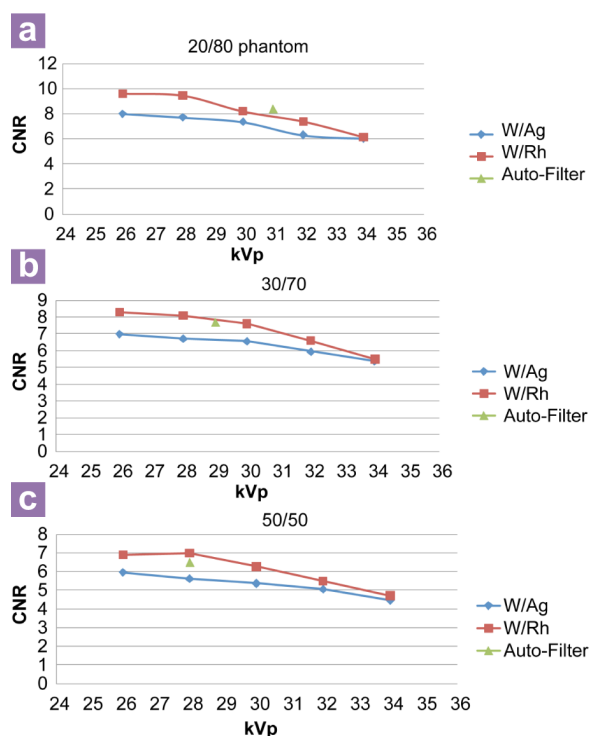


Figure 5: (a) The CNR value for 20/80 phantom, (b) the CNR value for 30/70 phantom, (c) the CNR value for 50/50 phantom.

The correlation between the AGD value of the TLD and ionization chamber (IC) is positive ($r = 0.846$, $P < 0.05$) and showed that the AGD value used for TLD-100H and the ionization chamber is in agreement. The AGD value using TLD and the ionization chamber displayed in table 1 showed that the maximum difference is at a high kVp for each phantom. The difference between TLD and IC is between 13–52%.

There is a strong correlation between the

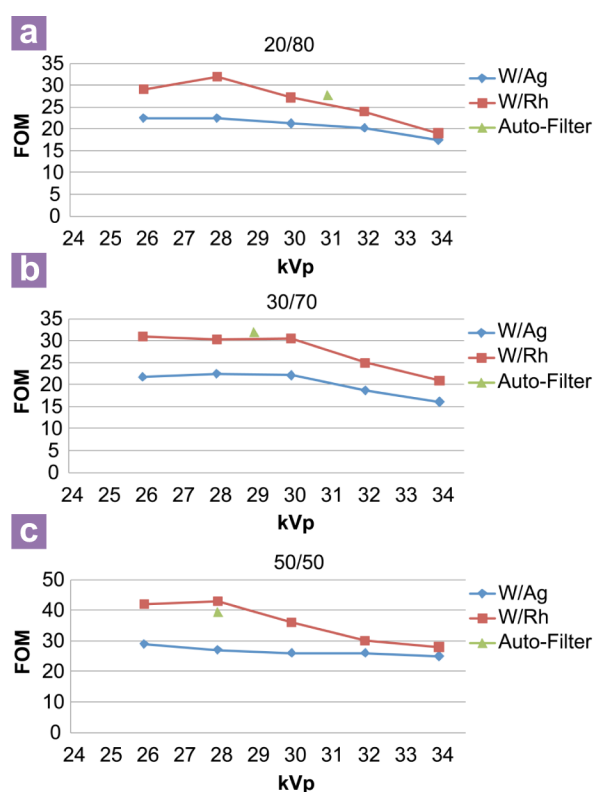


Figure 6: (a) The FOM value for 20/80 phantom, (b) the FOM value for 30/70 phantom, (c) the FOM value for 50/50 phantom.

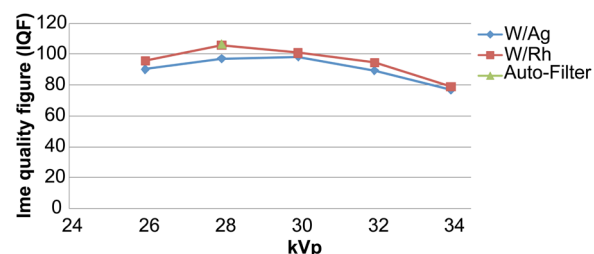


Figure 7: Image quality figure (IQF) versus tube output (kVp) shows the highest IQF, and the optimum tube potential is 28 kV with respect to all spectrums.

Table 1: Effect on dose, CNR and FOM of different mode of exposure for simulated breast phantom

| Exposure mode and phantom | Tube output (kVp) | mAs | Anode/filter | AGD TLD (mGy) | AGD IC (mGy) | CNR | FOM |
|---------------------------|-------------------|-----|--------------|-----------------|-----------------|-----------------|------------------|
| Auto-Time 20/80 | 26 | 225 | W/Ag | 2.84 ± 0.08 | 1.89 ± 0.01 | 7.99 ± 0.08 | 22.5 ± 0.48 |
| | 28 | 163 | W/Ag | 2.62 ± 0.08 | 1.44 ± 0.01 | 7.7 ± 0.26 | 22.48 ± 1.5 |
| | 30 | 114 | W/Ag | 2.6 ± 0.18 | 1.57 ± 0.01 | 7.3 ± 0.37 | 21.2 ± 0.89 |
| | 32 | 78 | W/Ag | 2.3 ± 0.06 | 1.41 ± 0.01 | 6.26 ± 0.3 | 20.2 ± 1.4 |
| | 34 | 54 | W/Ag | 2.09 ± 0.03 | 1.25 ± 0.01 | 6.05 ± 0.16 | 17.5 ± 0.93 |
| | 26 | 347 | W/Rh | 3.2 ± 0.03 | 2.56 ± 0.01 | 9.6 ± 0.3 | 29 ± 1.8 |
| | 28 | 228 | W/Rh | 2.82 ± 0.01 | 2.14 ± 0.01 | 9.45 ± 0.13 | 32 ± 0.89 |
| | 30 | 199 | W/Rh | 2.67 ± 0.14 | 1.97 ± 0.01 | 8.2 ± 0.3 | 27.2 ± 1.9 |
| | 32 | 142 | W/Rh | 2.28 ± 0.01 | 1.8 ± 0.02 | 7.4 ± 0.22 | 23.9 ± 0.78 |
| | 34 | 84 | W/Rh | 2.0 ± 0.18 | 1.3 ± 0.01 | 6.16 ± 0.14 | 19.02 ± 1 |
| Auto-Filter 20/80 | 31 | 171 | W/Rh | 2.44 ± 0.13 | 1.9 ± 0.01 | 8.42 ± 0.15 | 27.8 ± 1 |
| Auto-Time 30/70 | 26 | 112 | W/Ag | 2.2 ± 0.05 | 1.22 ± 0.01 | 6.98 ± 0.4 | 21.67 ± 4.2 |
| | 28 | 104 | W/Ag | 2.03 ± 0.08 | 1.08 ± 0.01 | 6.7 ± 0.25 | 22.49 ± 2.7 |
| | 30 | 77 | W/Ag | 1.89 ± 0.01 | 0.89 ± 0.01 | 6.55 ± 0.04 | 22.14 ± 0.31 |
| | 32 | 55 | W/Ag | 1.81 ± 0.4 | 0.78 ± 0.01 | 5.93 ± 0.04 | 18.7 ± 0.13 |
| | 34 | 31 | W/Ag | 1.65 ± 0.08 | 0.76 ± 0.01 | 5.39 ± 0.08 | 16.06 ± 0.27 |
| | 26 | 173 | W/Rh | 2.23 ± 0.04 | 1.57 ± 0.01 | 8.3 ± 0.12 | 31 ± 3.6 |
| | 28 | 164 | W/Rh | 2.17 ± 0.08 | 1.15 ± 0.01 | 8.09 ± 0.25 | 30.18 ± 1.8 |
| | 30 | 124 | W/Rh | 1.9 ± 0.11 | 1.09 ± 0.01 | 7.6 ± 0.06 | 30.5 ± 0.51 |
| | 32 | 78 | W/Rh | 1.77 ± 0.01 | 0.96 ± 0.01 | 6.6 ± 0.07 | 24.9 ± 0.32 |
| | 34 | 49 | W/Rh | 1.41 ± 0.18 | 0.63 ± 0.01 | 5.5 ± 0.15 | 21.4 ± 1.2 |
| Auto-Filter 30/70 | 29 | 53 | W/Rh | 1.78 ± 0.08 | 1.27 ± 0.01 | 7.7 ± 0.32 | 32.3 ± 1.74 |
| Auto-Time 50/50 | 26 | 80 | W/Ag | 1.24 ± 0.19 | 0.79 ± 0.01 | 5.96 ± 0.11 | 29.6 ± 0.24 |
| | 28 | 55 | W/Ag | 1.2 ± 0.04 | 0.75 ± 0.01 | 5.59 ± 0.24 | 26.6 ± 2.72 |
| | 30 | 65 | W/Ag | 1.11 ± 0.04 | 0.63 ± 0.01 | 5.35 ± 0.13 | 25.8 ± 1.28 |
| | 32 | 33 | W/Ag | 1.01 ± 0.15 | 0.57 ± 0.01 | 5.04 ± 0.23 | 25.2 ± 2.4 |
| | 34 | 23 | W/Ag | 0.76 ± 0.05 | 0.56 ± 0.01 | 4.47 ± 0.07 | 26.3 ± 0.8 |
| | 26 | 93 | W/Rh | 1.2 ± 0.01 | 0.94 ± 0.01 | 6.9 ± 0.08 | 39.5 ± 0.98 |
| | 28 | 96 | W/Rh | 1.16 ± 0.03 | 0.70 ± 0.01 | 7 ± 0.21 | 41.9 ± 3.1 |
| | 30 | 74 | W/Rh | 1.1 ± 0.03 | 0.71 ± 0.01 | 6.25 ± 0.29 | 33.7 ± 3.1 |
| | 32 | 52 | W/Rh | 1.0 ± 0.01 | 0.61 ± 0.01 | 5.5 ± 0.17 | 27.2 ± 1.7 |
| | 34 | 34 | W/Rh | 0.8 ± 0.03 | 0.62 ± 0.01 | 4.7 ± 0.15 | 27.7 ± 1.8 |
| Auto-Filter 50/50 | 28 | 91 | W/Rh | 1.16 ± 0.12 | 0.96 ± 0.01 | 6.5 ± 0.26 | 40.8 ± 1.8 |

Abbreviations: AGD = average glandular dose; CNR = contrast-to-noise ratio; FOM = figure of merit; W/Ag = Tungsten/Argentum; W/Rh = Tungsten/Rhodium.

Table 2: CDMAM image quality figure (IQF) for different types of exposure mode

| Mode of exposure | Tube output (kVp) | Anode/filter | IQF |
|------------------|-------------------|--------------|-------|
| Auto-Time | 26 | W/Ag | 90.1 |
| | 28 | W/Ag | 97 |
| | 30 | W/Ag | 98.3 |
| | 32 | W/Ag | 89.4 |
| | 34 | W/Ag | 77 |
| | 26 | W/Rh | 95.8 |
| | 28 | W/Rh | 105.9 |
| | 30 | W/Rh | 100.6 |
| | 32 | W/Rh | 94.6 |
| | 34 | W/Rh | 79.1 |
| AEC | 28 | W/Rh | 106.7 |

Abbreviations: W/Ag = Tungsten/Argentum; W/Rh = Tungsten/Rhodium; IQF = Image quality figure.

AGD (using TLD) with a CNR value for 20/80 breast phantom ($r = 0.804$), whereas for phantom 30/70, a moderate correlation was observed ($r = 0.5543$) and for phantom 50/50, moderate correlation ($r = 0.675$) was observed. It is shown that the CNR increases significantly when the AGD value increases.

The general linear model showed that the AGD value for all phantoms had a significant effect between different exposure factors [$F(6,12.3) = 4.48$] and mode of exposure [$F(1,86) = 4.17$, $P < 0.05$] but there is no significant difference between different the anode/filter combination [$F(1,4) = 0.571$].

Discussion

In particular, in the radiation dose between the tube output (kVp) for a lower kVp 26, 28, and 30, the Argentum filter has the lowest AGD compared with the Rh filter because the W/Ag combination produces more penetrating X-ray beams. These present a higher value of HVL and a lower value of AGD due to a minimum filter of 0.5 mm Ag, which is useful to attenuate the unwanted L X-rays (6).

The lower kVp of 26 and 28, in the auto-time mode, lengthened the exposure times for phantoms 20/80 and 30/70, respectively. The long exposure time of more than 4 s is impossible because it will increase the risk of hitting a back-up timer and terminating the exposure prematurely. Moreover, with a lower kVp, it may lengthen

the exposure time and increase the heat to the X-ray tube, and thus reducing the life-span of the X-ray tube. However, in the auto-filter mode, the exposure time is a short, thus preventing patient movement and blurring (15).

Although a high kVp (32–34) contributed to a lower radiation dose, it is important to investigate the image quality resulting from the exposure. In this study, FOM and the CDMAM phantom were used to assess image quality. Results reported in figure 5 and 6 showed that for each breast glandularity and anode/filter combination, the curves have a similar shape. As anticipated, subject contrast decreases with increasing kVp because of the decrease in the difference in the linear attenuation coefficients of the step-wedge and background materials (4). The CNR curves for W/Rh were higher compared with those for W/Ag. The CNR value, for a 6 cm thickness phantom has a higher CNR than a thinner phantom because of higher doses selected for thicker breasts (15). It is consistent with the statistical analysis that showed CNR increases as the AGD increases. In digital mammography, post-processing can be done to improve the contrast with changes in noise. Consequently, CNR is the best suited parameter to assess image quality objectively, since it shows how good the contrast is compared with the noise in a given image (16). However, the problem with CNR (and SNR) is that it is a system-dependent measurement, not only in terms of image processing but also when considering detector-related characteristics such as the pixel size (16).

Meanwhile this FOM, particularly the one defined in equation 3, is useful for investigations to compare the relative trade-off between the image quality and dose for a given imaging system when operational parameters are varied. The FOM has also been very useful in the assessment of AEC in mammography systems to ensure that the right exposure parameters are being selected for a specified breast thickness (17). The FOM should be independent of the dose level employed, given that the system used is quantum limited (6). If electronic or structural noise contributes to the total noise in addition to quantum noise, some results could be different. In this study, FOM values were higher for the 4 cm thickness phantom compared with the 6 cm thickness phantom (Figures 6a–6c). In particular, the FOM calculated for higher dose values could be lower. However, because the detector incorporated by the systems is the same, the comparison between the results is still valid (5).

It may be worth considering using a different

approach to the image quality analysis rather than CNR in defining the FOM, such as threshold contrast or the threshold contrast detectability index (17). One of the best methods to measure the quality objectively is the IQF. A comparison was made between the tube output and mode of exposure (auto-time and auto-filter) (Table 1). The curve for W/Rh was higher compared with that for W/Ag. In particular, W/Rh in the auto-time mode produces the highest IQF, and the optimum tube potential is 28 kV with respect to all spectrums (Figure 7). This result is consistent with FOM that it showed how a lower kVp obtained a higher score compared with a higher kVp, because a higher kVp will increase scatter radiation, thus reducing image contrast. Although 26 kVp was better in FOM, in terms of contrast and object detectability, it is lower than 28 kVp. The role of CDMAM in evaluating the quality of the image is well-known; nevertheless, by combining the results of the dose (from the CIRS phantom) and image quality measurements, optimum exposure factors could be calculated for each system as those that would enable it to reach the achievable image quality standard in the European Guidelines at the lowest dose (18).

The anode/filter combination with the W/Rh and W/Ag spectra, produced a better CNR and FOM for the lower kVp (28–30) with respect to all breast glandularity (Figures 5a–5c, and 6a–6c). The results obtained here are comparable with those from previous studies. For example, William et al. (4) stated that the SNR versus kVp curves for the two amorphous selenium FFDM systems Selenia and Mammomat Novation DR exhibited peaks around 26–29 kVp, with the SNR steadily falling with a decreasing kVp below the peak value, as well as with an increasing kVp above it. As far as the comparison of W/Rh and W/Ag is concerned, it is possible to achieve an increase in the FOM with an Rh filter, which correlates with the manufacturer's suggestion to use the Tungsten/Rh (W/Rh) combination for breast phantom thickness of 4 cm and less than 7 cm (19).

In particular, in the mode of exposure preference for phantom 50/50, the auto-filter mode showed comparable CNR and FOM values with 28 kVp selected, whereas for phantom 30/70, FOM was better with 29 kVp (auto-filter) compared with 28 kVp; therefore, 29 kVp is the optimum kVp for phantom 30/70. Hence, the auto-filter mode is suitable for 50% and 30% glandularity. Whereas for thicker and fatty tissues, in the 20/80 phantom, there is a 15% increase of the FOM value with 28 kVp in the auto-filter

mode, but with an increase of AGD for about 22%. If the kVp is 32, the FOM and AGD is 23.9 and 2.28 mGy, respectively, but the FOM and AGD decrease to about 14% and 6.6%, respectively, compared with the auto-filter mode. Because the CNR and FOM for the auto-filter mode is high compared with those for 32 kVp, it is better to choose the auto-filter mode with 31 kVp as the optimum kVp for the 20/80 phantom. Besides the CDMAM finding showed that in the auto-filter mode, the image has a higher contrast compared with the auto-time mode. Thus it is worth to use the auto-filter mode because it is automatic, faster, and easier for the operator task.

The correlation between the AGD value of the TLD and ionization chamber is strong and in agreement with the previous studies by Hobbs et al. and Wochos et al. (20, 21). The variation between the ionization chamber measurements and TLD measurements ranged from 4% to 24% in a study by Ng et al. (22), whereas in this study, it ranged from 13 to 52%. The readings are different between TLD and IC because of the TLD group itself, TLD reader, and calibration procedure. According to previous research, the uncertainty of the dose measurement is specified to be 12.98% because of different sources of uncertainty of the TLD badge and system (23). Apart from that, during the dosimetry with IC, the phantom was not present; thus there is a possibility that the dosage calculated is less than the actual dosage. Nevertheless, the diameter of the ionization chamber is thick to be put on the phantom, whereas the TLD size is thin, small, and equivalent to tissue material, and thus, it is easier to be put on the phantom. Moreover the IC reading is real-time, and thus, it is convenient and speeds up the dosimetry process.

There are a few limitations of this study. The CIRS breast phantom comes with specific glandularity and thickness, but it has superior image quality and detail; therefore, AGD was measured for specific breast thickness. In the future, further studies on the various thicknesses should be conducted.

Conclusion

In summary, slight changes in the tube output (± 1) could alter the radiation dose delivered to the patient and the image quality as well; however, the exposure factor should be modified only by an expert operator. The radiation dose to the breast does not only depend on kVp but also on mAs and the anode/filter combination. Therefore, the optimum kVp specific for each breast glandularity

should be identified in order to minimize the dose. In this study, the optimum tube output is 28, 29, and 31 kVp for 50%, 30%, and 20% breast glandularity, respectively. Besides the auto-filter mode is suitable for 50%, 30%, and 20% breast glandularity, respectively, because it is automatic, faster, and may avoid error created by the operator. The CNR increases when the AGD value is increased; therefore, factors such as kVp, filter, and compression should be optimised in a manner such that the lowest dose as possible is obtained without compromising the image quality (13).

Acknowledgement

The author would like to acknowledge grants MOHE, UKM-NN-07-FRGS0225 for funding this study. Sincere thanks to the staff at National Cancer Society Malaysia and Universiti Kebangsaan Malaysia for their cooperation and contribution for this study

Conflict of Interest

None.

Funds

These research was supported in part by the National University of Malaysia Research funding under grants MOHE, UKM-NN-07-FRGS0225-2010.

Authors' Contributions

Conception and design, analysis and interpretation of the data, drafting of the article: IK
Critical revision of the article for the important intellectual content, final approval of the article: KKC

Provision of study materials or patient: ST, VK

Correspondence

Prof Kanaga Kumari Chelliah
BAppSc (Curtin University), PG DIP (Edu) (Curtin University), MSc (Med Physics) (USM)
Diagnostic Imaging and Radiotherapy Programme
Faculty of Health Sciences
University Kebangsaan Malaysia
Jalan Raja Muda Abdul Aziz
50300, Kuala Lumpur
Malaysia
Tel: +603-2687 8101
Fax: +603-2687 8101
Email: kanagakkc@yahoo.com

References

1. Varjonen M, Strömmer P. Optimizing the anode-filter combination in the sense of image quality and average glandular dose in digital mammography. *Proc SPIE*. 2008;**6913**:69134K. doi: 10.1117/12.768083.
2. Mayo P, Rodenas F, Verdu G, Campayo JM, Villaescusa JI. Study of digital mammographic equipments by phantom image quality. *Conf Proc IEEE Eng Med Biol Soc*. 2006;**1**:1994–1996 doi: 10.1109/IEMBS.2006.259245.
3. Samei E, Dobbins JT, Lo JY, Tornai MP. A framework for optimising the radiographic technique in digital X-ray imaging. *Radiat Prot Dosim*. 2005;**114**(1–3):220–229. doi: 10.1093/rpd/nch562.
4. Williams MB, Raghunathan P, More MJ. Optimization of exposure parameters in full field digital mammography. *Med Phys*. 2008;**35**(6):2414–2423. doi:10.1118/1.2912177.
5. Williams MB, Raghunathan P, Seibert A, Kwan A, Lo JY, Samei E, et al. Beam optimization for digital mammography-II. *LNCS*. 2006;**4046**:273–280. doi: 10.1007/11783237_38.
6. Baldelli P, Phelan N, Egan G. Investigation of the effect of anode/filter materials on the dose and image quality of a digital mammography system based on an amorphous selenium flat panel detector. *Brit J Radiol*. 2010;**83**(988):290–295. doi: 10.1259/bjr/60404532.
7. Andrew S, Biao C, Alan S. *Minimizing dose in digital mammography*. Tungsten x-ray tubes with rhodium and silver filters optimize image quality [Internet]. Bedford (US): Hologic Inc; 2008 [cited 2011 Aug 18]. Available from: <http://www.hologic.com>.
8. Hammerstein GR, Miller DW, White DR, Masterson ME, Woodard HQ, Laughlin JS. Absorbed radiation dose in Mammography. *Radiology*. 1979;**130**(2):485–491. doi: 10.1148/130.2.485.
9. International Atomic Energy Agency (IAEA). Dosimetry in diagnostic radiology: an international code of practice Technical Reports Series no. 457 [Internet]. Vienna (AUT): IAEA; 2006 [cited 2012 Sept 12]. Available from: www.pub.iaea.org/MTCD/publications/PDF/TRS457_web.pdf.
10. Zeidan M. Assessment of Mean Glandular Dose in Mammography, Department of Physics and Astronomy [master's thesis]. [Christchurch (NZ)]: University of Canterbury; 2009.
11. Dance DR. Monte Carlo calculation of conversion factors for the estimation of mean glandular breast dose. *Phys Med Biol*. 1990;**25**(9):1211–1219. doi:10.1088/0031-9155/35/9/002.
12. Dance DR, Skinner CL, Young KC, Beckett JR, Kotre CJ. Additional factors for the estimation of mean glandular breast dose using the UK mammography dosimetry protocol. *Phys Med Biol*. 2000;**45**(11):3225–3240. doi: 10.1088/0031-9155/45/11/308.

13. Dance DR, Young KC, Van ER. Estimation of mean glandular dose for breast tomosynthesis: factors for use with the UK, European and IAEA breast dosimetry protocols. *Phys Med Biol*. 2011;**56**(2):453–471. doi: 10.1088/0031-9155/56/2/011.
14. Kanaga KC, Yap HH, Laila SE, Sulaiman T, Zaharah M, Shantini AA. A critical comparison of three full field digital mammography systems using figure of merit. *Med J Malaysia*. 2010;**65**(2):119–122.
15. Young KC, Ramsdale ML, Rust A, Cooke J. Effect of automatic kV selection on dose and contrast for a mammographic X-ray system. *Br J Radiol*. 1997;**70**(838):1036–1042. doi: 10.1259/bjr.70.838.9404208.
16. Poyry P. *Sentinel teaching course on digital mammography*. In: Proceedings of Optimisation of exposure settings in digital mammography. Finland (FR): STUK; 2006.
17. Borg M, Badr I, Royle GJ. The use of a figure-of-merit (FOM) for optimisation in digital mammography: A literature review. *Radiat Prot Dosim*. 2012;**151**(1):81–88. doi: 10.1093/rpd/ncr465.
18. Young KC, Cook JJH, Oduko JM, Bosmans H. Comparison of Software and Human Observers in Reading Images of the CDMAM Test Object to Assess Digital Mammography Systems. In: Proceedings of SPIE Medical Imaging. Bellingham (WA); SPIE Publications; 2006. p. 1–13. doi: 10.1117/12.653296.
19. Young KC, Oduko JM, Woolley L. Technical evaluation of the Hologic Selenia full field digital mammography system; NHSBSP equipment report 0701 January 2007 [Internet]. Sheffield (UK): NHS Cancer Screening Programmes; 2007 [cited 2012 Dec 20]. Available from: www.cancerscreening.nhs.uk.
20. Hobbs T. Response comparison of electret ion chambers, LiF TLD, and HPIC. *Radiat Prot Dosimetry*. 1996;**63**(3):181–188.
21. Wochos JF, Fullerton GD, DeWerd LA. Mailed thermoluminescent dosimeter determination of entrance skin exposure and half-value layer in mammography. *Am J RoentgenoL*. 1978;**131**(4):617–619.
22. Ng KH, DeWerd LA, Schmidt R. Mammographic image quality and exposure in South East Asia. *Australas Phys Eng Sci Med*. 2000;**23**(4):135–137.
23. Rabie N, Hany A, Shousha GM, Hassan. Achievement of quality control parameters for NIS personal thermoluminescence dosimeter (TLD) system. *J Basic Appl Sci Res*. 2011;**7**:548–543.